Simulations of iron K pre-edge X-ray absorption spectra using the restricted active space method†

Meiyuan Guo,[a] Lasse Kragh Sørensen,[a] Mickaël G. Delcey,[a,b] Rahul V. Pinjari,[a,c] and Marcus Lundberg*[a]

The intensities and relative energies of metal K pre-edge features are sensitive to both geometric and electronic structure. With the possibility to collect high-resolution spectral data it important to find theoretical methods that include all important spectral effects: ligand-field splitting, multiplet structures, 3*d*-4*p* orbital hybridization, and charge-transfer excitations. Here the restricted active space (RAS) method is used for the first time to calculate metal K pre-edge spectra of open-shell systems, and its performance is tested against six iron complexes: $[FeCl_6]^{n-}$, $[FeCl_4]^{n-}$, and $[Fe(CN)_6]^{n-}$ in ferrous and ferric oxidation states. The method gives good descriptions of the spectral shapes for all six systems. The mean absolute deviation for the relative energies of different peaks is only 0.1 eV. For the two systems that lack centrosymmetry $[FeCl_4]^{2-/1-}$, the ratios between dipole and quadrupole intensity contributions are reproduced with an error of 10%, which leads to good descriptions of the integrated pre-edge intensities. To gain further chemical insight, the origins of the pre-edge features have been analyzed with a chemically intuitive molecular orbital picture that serves as a bridge between the spectra and the electronic structures. The RAS method can thus be used to predict and rationalize the effects of changes in both oxidation state and ligand environment in a number of hard X-ray studies of small and medium-sized molecular systems.

1 Introduction

X-ray absorption spectroscopy (XAS) is a powerful technique to study structure and function of transition metal sites.[1] For K-edge XAS (1*s* excitations) of first-row transition metals, the incident photon is in the hard X-ray regime and the absorption spectrum can be obtained *in situ*, which makes it possible to study enzymatic systems and working catalysts.[2–5] The K pre-edge directly probes the unoccupied and partially occupied valence orbitals involved in catalysis and can play a key role in the identification and characterization of reactive sites, e.g., site symmetry, oxidation state and ligand-field splitting.[6–10] Westre and co-workers analyzed the iron K pre-edges for a large series of systems, both experimentally and theoretically. They showed how energy and intensity depend on oxidation state and coordination number, and provided a general method for their interpretation.[7] The K pre-edge has already been very useful in geometry and electronic structure analysis, such as determining the protonation state of a ferryl intermediate[9] and the coordination number of a non-heme iron active site.[10]

For centrosymmetric complexes, the K pre-edges are associated with electron transitions from the 1*s* to the 3*d* orbitals. These are electric quadrupole transitions that have very weak intensity compared to the electric dipole-allowed 1*s* to 4*p* K-edge transitions, ∼2 orders of magnitude weaker.[11] The intensity of the K pre-edge increases significantly if the centrosymmetric environment is broken, *e.g.*, when going from a six-coordinate to a five-coordinate site.[7] Distortions from centrosymmetry allow for 4*p* orbital character to mix into metal-3*d* orbitals through their mutual interactions with the ligand orbitals. This 3*d*-4*p* orbital hybridization is an important intensity mechanism as it gives rise to dipole-allowed transitions in the pre-edge. The amount of mixing between 3*d* and 4*p* largely depends on the site symmetry and can be interpreted using group theory.[12] Que and co-workers showed that the iron K pre-edge intensity has a near linear correlation with the total amount of 4*p* orbitals in the 3*d*-type molecular orbitals.[10,13] It is thus essential to be able to estimate the dipole contributions when a catalyst site changes during a reaction.

In many open-shell systems, the pre-edge excitations lead to a large number of different final states. The multiplet structure formed by differences in electron-electron correlation can give detailed information about the electronic structure. However, the metal K pre-edge features are not well resolved due to the short lifetime of the 1*s* core hole, which gives a large natural bandwidth (∼1.25eV for *Fe*).[14] One possible solution is to use resonant inelastic X-ray scattering (RIXS), because the resolution in the energy transfer direction is affected only by the lifetime of the final state, not the lifetime of the 1*s* core hole in the intermediate state.[15]. Recently, high-resolution

0† Electronic Supplementary Information (ESI) available: See DOI: 10.1039/b000000x/

0[a] *Department of Chemistry-Ångström laboratory, Uppsala University, SE-751 20 Uppsala, Sweden.; E-mail: marcus.lundberg@kemi.uu.se.* [b] *Present address: Chemical Sciences Division, Lawrence Berkeley National Laboratory, Berkeley, California 94720, USA and Kenneth S. Pitzer Center for Theoretical Chemistry, Department of Chemistry, University of California, Berkeley, California 94720, USA.* [c] *Present address: School of Chemical Sciences, Swami Ramanand Teerth Marathwada University, Nanded 431606, Maharashtra, India.*

resonant inelastic X-ray scattering (RIXS) spectra have been used to get detailed electronic structure information, *e.g.* the $3d$ orbital covalency and $3d-3d$ excitation, using hard X-rays.[16–19] With RIXS experiments reaching 0.1 eV resolution direction in the energy transfer direction,[20] it becomes important to include both multiplet effects and charge-transfer states in the analysis.[18]

X-ray spectra that only involve $1s$ core holes can be described by a number of different approaches.[21–27] Time-dependent (TD) density-functional theory (DFT) has been used to model transition-metal K pre-edge absorption spectra.[28–30] This provides a framework for the calculation of $1s$ to $3d$ transition energies and intensities with a very favourable balance between accuracy and computational time. It also naturally includes dipole contributions due to distortions from centrosymmetry.[28] Limitations are that it does neither correctly account for multiplet effects, arising from electron−electron correlations, nor mutiple excitations such as core hole induced charge transfer processes. In addition, the energies of direct charge-transfer excitations are usually underestimated for highly covalent complexes.[31–33].

For experiments with important multiplet effects, one attractive possibility is to use the semi-empirical charge-transfer multiplet (CTM) model.[34] This method includes all relevant final states and gives a a balanced description of electron-electron correlation and spin-orbit coupling (SOC). For symmetric systems it often achieves excellent agreement with experimental data through a multi-parameter fit to the experimental spectrum.[35–37] However, the number of model parameters increases with decreasing symmetry. Moreover, additional parameters are required to describe the $3d$-$4p$ orbital hybridization.[38] This makes it more complicated to apply the CTM model for complexes with little or no symmetry.

Thus, a method is required that accurately describes electron correlation and orbital hybridization without fitting parameters. One solution is to use a multi-configurational self consistent field (MCSCF) approach, such as the restricted active space (RAS) SCF method.[39] This has previously been used to model L-edge XAS spectra of several transition-metal systems.[40–42] In these calculations, the important valence orbitals are included in an active space where all excitations are allowed. The core orbital is also included in the active space, but the number of excitations is restricted to one, which gives the RAS approach. In a second step, dynamical correlation is included using second-order perturbation (RASPT2).[43] To provide chemical insight, a method has been designed to extract spectral contributions in the form of a chemically intuitive molecular orbital picture.[41]

The RAS methodology will now be used for the first time to model transition-metal K pre-edges of open-shell systems. The goal is to understand the accuracy and applicability for a series of well-known model complexes, before applying it to systems with unknown electronic or geometric structure. First, the K pre-edge spectra of the high-spin O_h symmetric ferric/ferrous hexachloride ($[FeCl_6]^{3-}$ and $[FeCl_6]^{4-}$), see Fig. 1, are compared to highlight multiplet structures and ligand-to-metal charge transfer (LMCT) states. Next, mixing of dipole and quadrupole transitions is tested for two tetrahedral complexes, ferrous/ferric tetra-chloride ($[FeCl_4]^{1-}$ and $[FeCl_4]^{2-}$), see Fig. 1. Finally, simulations of the low-spin ferrous/ferric hexa-cyanide systems ($[Fe(CN)_6]^{4-}$ and $[Fe(CN)_6]^{3-}$) are done to understand the potential to directly measure π back-donation. Together, these complexes test the performance of the RAS method for a number of different bonding situations, oxidation states and ligand environments. Whenever possible, the results are compared to those from CTM, and previously published TD-DFT results,[28] to throughly understand the performance of the computational methods.

2 Computational details

State-average RASSCF and multi-state RASPT2 calculations have been performed with a development version of MOLCAS.[44] The active space is designated as RAS(n, l, m; i, j, k), where i, j, and k are the number of orbitals in RAS1, RAS2, and RAS3 spaces respectively, n is the total number of electrons in the active space, l the maximum number of holes allowed in RAS1, and m the maximum number of electrons in RAS3. For all systems, the important valence orbitals are included in RAS2, where all possible excitations are allowed. The $1s$ orbital is included in RAS3, with a single excitation allowed. Orbital optimization has been performed separately for ground and excited states. For the calculations of the excited states, the weights of all configurations with a doubly occupied 1s orbital have been set to zero. To avoid orbital rotation, i.e., that hole appears in the $3s$ instead of the $1s$ orbital, the latter has been frozen in the orbital optimization of the final states.

For all systems, the valence active space includes the metal-$3d$ dominated molecular orbitals t_2 and e. For $[FeCl_6]^{3-}$ and $[FeCl_6]^{4-}$ two ligand-dominated filled σ orbitals are added to the active space, together with empty $4d$ t_{2g} orbitals that are included for correlation,[45] which gives a total of 10 valence orbitals, see Fig. 1. This corresponds to RASPT2(11,0,2;0,10,1) and RASPT2(12,0,2;0,10,1) for the ferric and ferrous systems. For $[FeCl_4]^{1-}$ and $[FeCl_4]^{2-}$ the active space includes three ligand-dominated filled π (t_2) orbitals, as well as two empty sets of t_2 orbitals, see Fig. 1, giving RASPT2(13,0,2;0,11,1) and RASPT2(14,0,2;0,11,1). In the modeling of $[Fe(CN)_6]^{3-}$ and $[Fe(CN)_6]^{4-}$, two filled ligand-dominated σ orbitals and three empty ligand-centered antibonding (π^*) orbitals are included, giving RASPT2(12,0,2;0,10,1) and RASPT2(11,0,2;0,10,1) respec-

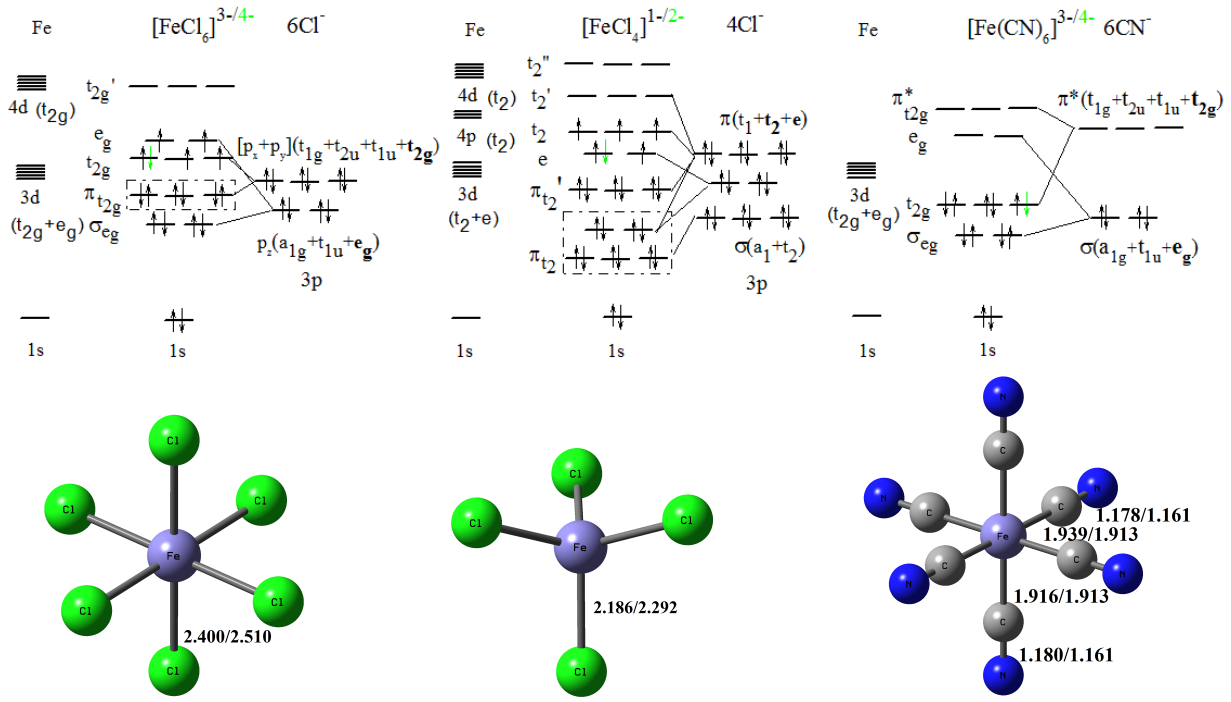

Fig. 1 Schematic molecular orbital diagrams and structures for the six ferrous d^6 and ferric d^5 iron complexes. The active spaces includes all represented molecular orbitals, except those within the dashed boxes. Bond distances for ferric/ferrous complexes are given in Å. The extra electrons in the ferrous complexes are marked with green arrows.

tively. Selected active orbitals in the ground and excited states are available in the Supporting Information (SI) Figs. SI1-SI6.

The orbital optimization depends on the number of states in the state-average RASSCF calculations. The number of states were chosen by monitoring the spectra until no significant changes could be detected, see Figs. SI7-SI9. In the final state this gave 30 states per irreducible representation for $[FeCl_6]^{3-}$, $[FeCl_4]^{1-}$ and $[FeCl_4]^{2-}$, and 20 states for $[FeCl_6]^{4-}$ and $[Fe(CN)_6]^{4-}$, while $[Fe(CN)_6]^{3-}$ required 80 states. Spin-flipped final states have negligible contributions to the K pre-edge spectra and all excited state calculations have been performed using the same spin multiplicity as the ground state.

Scalar relativistic effects have been included by using a Douglas-Kroll (DK) Hamiltonian in combination with a relativistic atomic natural orbital basis set, ANO-RCC-VTZP.[46,47] A density-fitting approximation of the electron repulsion integrals has been used, using auxiliary basis sets from an atomic-compact Cholesky decomposition.[48,49] Calculations have been performed using the default ionization-potential electron-affinity shift of 0.25 hartree,[50] and to reduce problems with intruder states an imaginary shift of 0.3 hartree has been applied.[51]

Oscillator strengths have been calculated between orthogonal states formed from a RAS state-interaction approach that also includes spin-orbit coupling. Intensities for quadrupole transitions have been calculated using a local implementation of the origin-independent second-order expansion of the wave vector.[52] A detailed analysis of the different contributions is given in Table SI1. Vibronic effects are expected to be small and have been neglected.[28]

Simulations have been performed using the ground state geometries,[53–57] see Fig. 1. Details are available in the Table SI2.

The cost of K pre-edge XAS calculations are slightly higher than for standard ground-state calculations, due to both the inclusion of core orbitals in the active space and the large number of final states.[42]

Semi-empirical CTM calculations are performed with the CTM4XAS program,[34] using parameters originally fitted to reproduce L-edge spectra.[35,36] A list of parameters for all multiplet simulations is given in Table SI3. TD-DFT results are taken directly from reference[28]. They were obtained with the BP86 functional[58,59] level using the CP(PPP) basis set[60] on *Fe* and TZVP on the remaining atoms. The metal-ligand orbital have also been calculated using B3LYP[61] with TZVP basis set,[62] the covalency analyses are performed using Multiwfn package.[63]

Comparisons with experimental K-edge spectra are done using data from reference[7], see Fig. SI10. Spectra were normalized to an edge jump of 1 at 7130 eV and energies were

calibrated using an iron foil, assigning the first inflection point to 7111.2 eV. The integrated experimental pre-edge areas are taken directly from the original publication.[7] In that study the peak areas were approximated by the height times the full-width half-maximum (in eV) of the Pseudo-Voigt peaks, and then been multiplied by 100 to get numbers that are easy to read. This is reported as the integrated pre-edge area. To facilitate visual comparisons of simulated and experimental pre-edges, new fits to the experimental spectra were made using EXAFSPAK,[64] after which the rising edges were subtracted from the original data, see Fig. SI11-SI13.

Simulated core RAS and CTM spectra are plotted using a Lorentzian broadening with a full-width-at-half-maximum (FWHM) of 1.25 eV and further convoluted with Gaussian broadening of 1.06 eV.[14] The energies of the calculated spectra are shifted to align with the experimental spectra at the first intense transition. The intensities of the simulated spectra have been scaled to the integrated intensity of the edge-subtracted experimental spectra. Here the same scaling factor has been used for all six systems, see Table SI4. The spectra have been analyzed using a chemically intuitive molecular orbital picture, where the changes in orbital occupation numbers during a transition are multiplied by the intensity of that particular transition. For details see reference[41]. Values above and below the x axis represent addition and depletion of the electron density in the respective orbitals.

3 Results and discussion

3.1 Multiplet structure

$[FeCl_6]^{3-}$ and $[FeCl_6]^{4-}$ are high-spin systems with σ and π donor ligands, see Fig. 1. The K pre-edge of $[FeCl_6]^{3-}$ has two peaks at 7112.8 and 7114.0 eV, see Fig. 2. The intensity ratio between the two peaks is 3.7:2.0, see Table 1. The $[FeCl_6]^{4-}$ spectrum also appears to have two pre-edge peaks, but a closer analysis reveals two close-lying peaks (at 7111.3 and 7111.8 eV), followed by a third peak at higher energy (7113.4 eV).

$[FeCl_6]^{3-}$has a $t_{2g}{}^3e_g{}^2$ ($^6A_{1g}$) ground state configuration. The two peaks can be rationalized in a simple ligand-field picture. Excitation of a 1s electron to either a t_{2g} or an e_g orbital gives two possible valence electron configurations, $^5T_{2g}$ and ^5E_g. Including also the spin of the core hole, both are sextet states, but considering only valence electrons makes it possible to use the familiar terminology for valence excited states. These states are split by 3d spin-orbit coupling, but that does not significantly affect the energies. The peak separation of 1.2 eV is therefore a direct probe of the ligand-field strength in this system. , All three theoretical methods correctly describe this simple two-transition system. In RAS the energy difference between the two states is ∼1.3 eV, with corresponding values for CTM and DFT calculations of 1.2 and 0.8 eV.

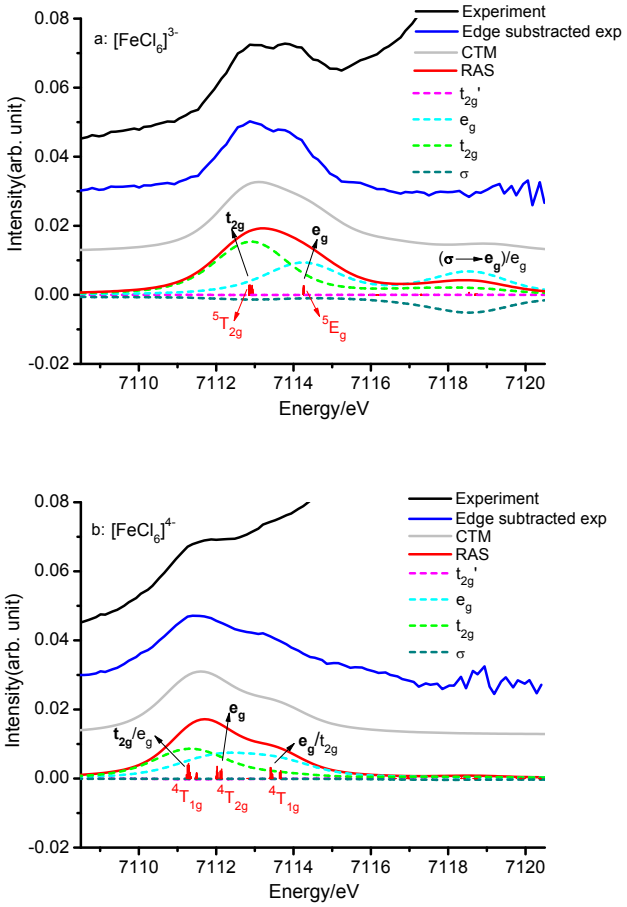

Fig. 2 Iron K pre-edge XAS spectra of (a) $[FeCl_6]^{3-}$ and (b) $[FeCl_6]^{4-}$ showing experimental data (black), the edge-subtracted spectra (blue), results from CTM calculations (light gray), and results from core RAS calculations (red). Analyses of the valence orbital contributions are shown as dashed lines. The characters of each peak are dominated by the excitations in bold, here electron from 1s orbital is omitted.

The RAS orbital analysis confirms that these are pure t_{2g} and e_g transitions, see Fig. 1a. The RAS calculation also gives a good estimate (3.5:2.0) of the intensity ratio of the two peaks (3.7:2.0 in experiment), see Table 1. By accounting only for the number of holes in the t_{2g} and e_g orbitals, the expected intensity ratio would be 3.0:2.0, but covalent interactions between metal and ligands orbitals decreases the metal 3d character and consequently the quadrupole intensity. As the t_{2g} orbitals are less covalent than the e_g orbitals, the $^5T_{2g}$ peak is less affected and becomes relatively more intense.

Calculated metal-ligand covalencies from the three different methods are given in Table SI5. RAS gives rather ionic results, 98% for t_{2g} and 83% for e_g, more ionic than both CTM

Table 1 Energies (in eV) and integrated intensities of pre-edge features from experiment and theory. Spectra are aligned at the first peak, with energy shifts listed in Table SI4.

	Experiment[a]	RAS	CTM[d]	TD-DFT[e]
$[FeCl_6]^{3-}$				
E1(int)	7112.8(2.6)	-	-	-
E2(int)	7114.0(1.4)	7114.1	7114.0	7113.6
E3(int)	-	7118.3	7118.7	-
ratio[b]	3.7:2.0	3.5:2.0:0.7	3.4:2.0:0.4	-
$[FeCl_6]^{4-}$				
E1(int)	7111.3(1.2)	-	-	-
E2(int)	7111.8(1.8)	7111.9	7112.1	7112.3
E3(int)	7113.4(0.6)	7113.4	7113.5	-
ratio[b]	2.0:3.0:1.0	1.8:0.9:1.0	1.8:1.0:1.0	-
$[FeCl_4]^{1-}$				
E1(int)	7113.2(20.7)	-	-	7113.2
E2(int)	-	7116.6	-	-
D/*Q* ratio[c]	3.2:1.0	3.5:1.0	-	7.0:1.0
$[FeCl_4]^{2-}$				
E1(int)	7111.6(8.6)	-	-	-
E2(int)	7113.1(4.3)	7113.1	-	7112.3
D/*Q* ratio[c]	2.3:1.0	2.4:1.0	-	7.5:1.0
$[Fe(CN)_6]^{4-}$				
E1(int)	7112.9(4.2)	-	-	-
E2(int)	-	7115.6	7115.1	7113.5
ratio[b]	-	2.0:1.0	4.0:1.0	-
$[Fe(CN)_6]^{3-}$				
E1(int)	7110.1(1.0)	-	-	-
E2(int)	7113.3(4.1)	7113.3	7113.4	7113.6
E3(int)	-	7117.3	7117.1	7115.2
ratio[b]	1.0:4.1	1.0:4.2:1.6	1.0:4.4:0.2	-

[a] Energies and integrated pre-edge intensities (x100) from reference [7].
[b] Intensity ratio between peaks.
[c] Ratio between electric dipole (*D*) and electric quadrupole (*Q*) contributions.
[d] CTM results with parameters from Table SI3.
[e] TD-DFT results (BP86 functional) from reference [28].

and DFT (BP86). This is expected as the RASSCF procedure typically leads to orbitals that are ionic in character, and these orbitals are not corrected in the perturbation treatment of dynamical correlation. Taking only the orbital covalency and number of holes into account, this gives directly the 3.5:2.0 ratio of the calculated RAS spectrum. The pre-edge intensities of high-spin d^5 systems should thus be able to probe metal-ligand covalency. The effects of covalency on the integrated intensity have previously been discussed for the L-edge XAS spectrum. [35]

In the RAS and CTM calculations there is also a third peak, located 4-5 eV above the e_g resonance. The orbital analysis, see Fig. 2a, suggests that this is a $1s \rightarrow 3d$ excitation, combined with a ligand σ to metal e_g transition. This spectral feature can thus be assigned as a shake-up transition of ligand-to-metal charge-transfer (LMCT) nature, similar to the feature seen in in the L-edge XAS spectrum. [35,41] This feature would be a direct probe of the ligand orbitals, but has not been identified in the current K-edge spectrum. With better statistics it could be possibly to separate it from the intense rising edge.

The pre-edge of $[FeCl_6]^{4-}$ is slightly more complicated than for the ferric system. Three features can be resolved experimentally, two states separated by 0.5 eV and then third state 2.1 eV above the first. [7] With a ground-state electron configuration of $t_{2g}{}^4 e_g{}^2$, an excitation from $1s$ to t_{2g} gives a single $^4T_{1g}$ state (considering only the d^7 valence state). An excitation to e_g instead gives rise to two different states, $^4T_{2g}$ and $^4T_{1g}$, split by $3d$-$3d$ interactions.

The RAS model has all three peaks, split by 0.6 and 2.1 eV, and an overall spectral shape that is in good agreement with experiment, see Fig. 2. No high-energy LMCT feature is predicted, which is in line with the observations from L-edge XAS spectra. [35,41] The difference between the two e_g final states is most easily seen by considering a wavefunction where the fourth t_{2g} electron is in the d_{xy} orbital. In that case the $^4T_{2g}$ state has the third e_g electron in the d_{z2} orbital, while in the $^4T_{1g}$ state it is in the d_{x2-y2} orbital, see Fig. 3., the wave-

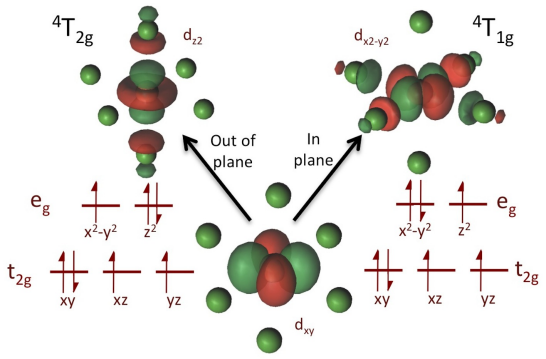

Fig. 3 The occupation of high spin d^6 system after $1s \rightarrow 3d(e_g)$ excitation.

functions of are $^4T_{1g}$ and $^4T_{2g}$ states available in Fig. SI14. In the latter case, the two orbitals are in the same plane, leading to a larger electron-electron repulsion than if the orbitals are in different planes. The energy difference can be used as an indirect measure of orbital covalency, because higher covalency decreases the d-d repulsion, and thus the energy difference between the two e_g states. The picture is slightly more complicated as the two $^4T_{1g}$ states can mix. This is visible in the orbital contribution analysis where the two peaks include contributions from both t_{2g} and e_g orbitals, see Fig. 2. This interaction splits the two $^4T_{1g}$ states, so the relative energies reflect three factors, the ligand field, the orbital covalency and the amount of configuration interaction. RAS includes all these three factors, which explains the good performance when it comes to the shape of the pre-edge. The CTM results are in good agreement with those from RAS, while TD-DFT has only two peaks separated by $\sim$1.0 eV. [28]. It is not unexpected that TD-DFT has problems for a system with both

strong multiplet effects and configuration interaction between the two $^4T_{1g}$ states.

For the ferric complex, the relative pre-edge intensities could be used to probe covalency, and were well described by RAS. For the ferrous complex, the experimental ratio between t_{2g} and e_g final states is 2:4, far from the ratio determined by the number of holes (2:2). This deviation cannot be explained by differences in covalency. Both RAS and CTM simulations give ratios that closely match the number of holes. One possibility is that the individual peak intensities are too sensitive to the K pre-edge fitting procedure, and it is therefore difficult to use these numbers to estimate the covalencies.

3.2 Dipole and quadrupole contributions

As mentioned in the introduction, breaking the centrosymmetry can lead to a significant increases in pre-edge intensity.[7,11] Here $[FeCl_4]^{1-}$ and $[FeCl_4]^{2-}$ are used as examples. They are higly symmetric (T_d) but lack an inversion center. The experimental K pre-edge spectrum of $[FeCl_4]^{1-}$ has a single intense peak at 7113.2 eV while $[FeCl_4]^{2-}$ has two peaks at 7111.6 and 7113.1 eV, see Fig. 5. Compared to the hexa-coordinated complexes, the total pre-edge intensity increases 5.2 times for the ferric and 3.6 times for ferrous complexes, see Fig. SI10. These enhancements in total intensity come from the presence of electric dipole-allowed transitions in the pre-edge. The dipole to quadrupole ratio is 3.2:1.0 for $[FeCl_4]^{1-}$, and 2.3:1.0 for $[FeCl_4]^{2-}$,[7] see Table 1 and Fig. 4.

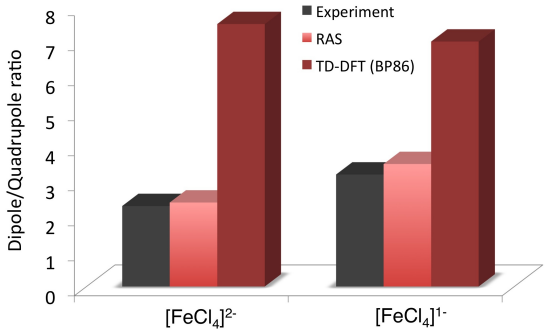

Fig. 4 The ratio of dipole to quadrupole contributions from experiment, RAS and TD-DFT.

$[FeCl_4]^{1-}$ has an $e^2t_2{}^3$ electronic configuration, which gives a $^6A_1$ ground state. As for the six-coordinated ferric complex, there are two one-electron excited valence configurations, $e^3t_2{}^3$ and $e^2t_2{}^4$, giving ^5E and $^5T_2$ valence states. However, the spectrum is dominated by one of these transitions, the t_2 one. This can be explained by the intense dipole contribution, see Fig. 5, which comes from the mixing of $4p$ orbitals (t_2 symmetry) with metal $3d$ t_2 orbitals through interactions with the ligands.[12]

The RAS calculations gives a decent estimate for the intensity ratio between $[FeCl_4]^{1-}$ and $[FeCl_6]^{3-}$, 4.6 compared to 5.2 in experiment. The ratio of dipole to quadrupole contributions is also good, 3.5:1.0 compared to 3.2:1.0 in experiment, see Table 1 and Fig .4. This is a significant improvement compared to the DFT result of 7.0:1.0. These numbers are very sensitive to the amount of $4p$ character in the valence orbitals.[7,10,13,65] Looking at the RAS orbitals, each t_2 orbital of $[FeCl_4]^{1-}$ has 1.1% $4p$ character, see Table SI5. For all three orbitals this gives a total $4p$ contribution of 3.3%. In the B3LYP calculations the total $4p$ contribution is 7.8%, similar to the previously reported local density approximation (LDA) results of 7.5%.[7] As expected, a lower $4p$ contribution also gives a smaller dipole/quadrupole ratio and, at least in this system, RAS gives the best agreement with experiment.

The RAS calculation of $[FeCl_4]^{1-}$ also predicts a shake-up feature, similar to what was previously seen for $[FeCl_6]^{3-}$. Here it is $1s \rightarrow t_2$ excitation, combined with a π to t_2 LMCT process, see Fig. 5. The electric dipole contributions give this transition a non-negligible intensity, and the peak fit shows a minor feature in this energy region, see Fig. SI12.

From a high-quality pre-edge spectrum it should thus be possible to see three peaks. The energy difference between the first two probes the ligand-field splitting, while the energy difference between the last two probes the ligand orbital energies. The pre-edge intensity depends more on the amount of $4p$ mixing than the covalency, and is a sensitive measure of the coordination environment.

The K pre-edge of $[FeCl_4]^{2-}$ looks different from the ferric counterpart with two intense peaks split by 1.5 eV.[7] The ^5E ground state has a $e^3t_2{}^3$ configuration and the first transition to the e orbital gives a $e^4t_2{}^3$ $^4A_2$ state with only electric quadrupole contributions. A t_2 excitation gives $^4T_2$ and $^4T_1$ states, which both have electric dipole contributions, and therefore should dominate the pre-edge shape. As discussed previously for the hexa-chloride complex, the energy difference between these states depends on the differences in electron repulsion between d orbitals, most easily represented as a difference in repulsion between electrons in d_{xy} and the out-of-plane d_{z2} orbital compared to the in-plane d_{x2-y2} orbital.

The RAS calculation gives good estimates of both the ratio between $[FeCl_4]^{2-}$ and $[FeCl_6]^{4-}$ pre-edge intensities (3.2:1.0 vs. 3.6:1.0 in experiment) and the ratio between electric dipole/quadrupole contributions (2.4:1.0 vs. 2.3:1.0 in experiment), see Fig .4. The calculated pre-edge has two main pre-edge features, split by 1.5 eV, just as in experiment, see Table 1. However, these are not simply the two intense dipole transitions expected from the ligand-field picture. Instead there are two different $^4T_1$ transitions, see Fig. 5. The second $^4T_1$ configuration represents a double excitation, giving $e^2t_2{}^4$, but the two configurations mix strongly as seen from the orbital analysis in Fig. 5.

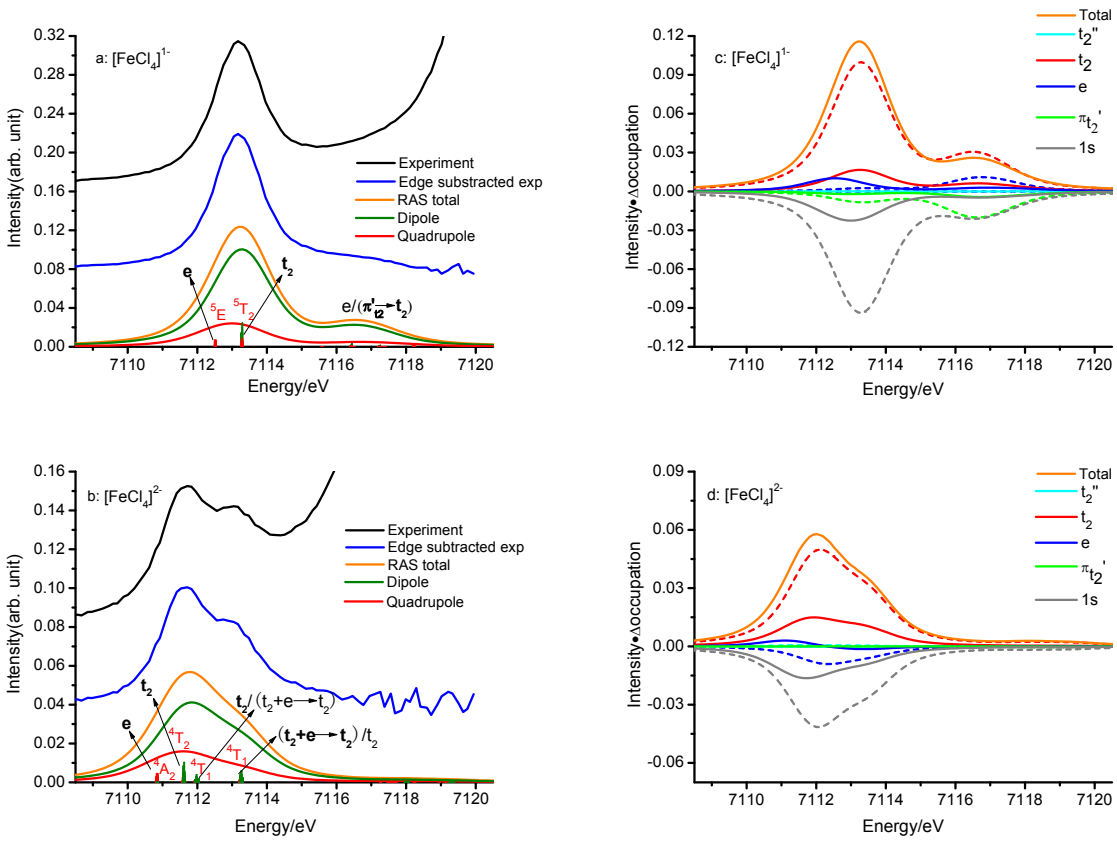

Fig. 5 Left:Iron K pre-edge XAS spectra of (a) $[FeCl_4]^{1-}$ and (b) $[FeCl_4]^{2-}$ showing experimental data (black), the edge-subtracted spectra (blue), and RAS results (total:orange, dipole:olive, quadrupole:red). Right:Orbital analyses for the K pre-edge XAS spectra of (a) $[FeCl_4]^{1-}$ and (b) $[FeCl_4]^{2-}$. Quadrupole contributions are denoted with solid lines while dipole contributions are shown with dashed lines.

For $[FeCl_4]^{2-}$, the pre-edge energies has information about both ligand-field splitting and orbital covalency, but for a correct interpretation, the effects of configuration interaction with a doubly-excited state needs to be accounted for. The intensity is mainly sensitive to the amount of $4p$ mixing. The RAS simulations includes all these effects and can therefore be used to disentangle these effects and give a coherent description of the electronic structure.

3.3 Probing back-donation

$[Fe(CN)_6]^{4-}$ and $[Fe(CN)_6]^{3-}$ have been widely used as π back-donation model systems.[18,36,37] In the L-edge XAS spectra, both complexes have intense peaks that can be assigned to back-donation. However, it is not clear whether such features can be detected in K pre-edge spectra.

For the two cyanide complexes, the analysis starts with the ferrous, instead of the ferric complex, because the pre-edge is simpler with a single visible peak at 7112.9 eV, see Fig. 6. In ferrocyanide the three t_{2g} orbitals are filled with six electrons giving a ${t_{2g}}^6{e_g}^0$ configuration with ${}^1A_{1g}$ symmetry. The pre-edge peak can therefore only come from an excitation to the e_g orbitals, producing a $t_{2g}^6 e_g^1$ configuration.

The RAS calculation has the main e_g transition, but more interestingly, it also has a second peak 2.7 eV higher in energy. Looking at the edge-subtracted experimental spectrum, it also has a peak with significant intensity 2.7 eV above the first one, see Fig. 6. An orbital analysis shows that the peak comes from excitations into empty π^* orbitals that are consequences of π back-bonding, i.e., a direct metal-to-ligand charge transfer, see Figs. 1 and 6. This assignment is supported by a simulation without the three π^* orbitals in the active space, where the peak has disappeared, see Fig. SI15. RAS predicts the position of this peak better than any other method. In the CTM calculations it has lower intensity and is located 1.9 eV above the e_g transition, while TD-DFT underestimates the energy and places it only 0.6 eV above the main peak.[28] The main issue with the RAS simulation is that the total intensity seems to be underestimated, but this will be discussed in more

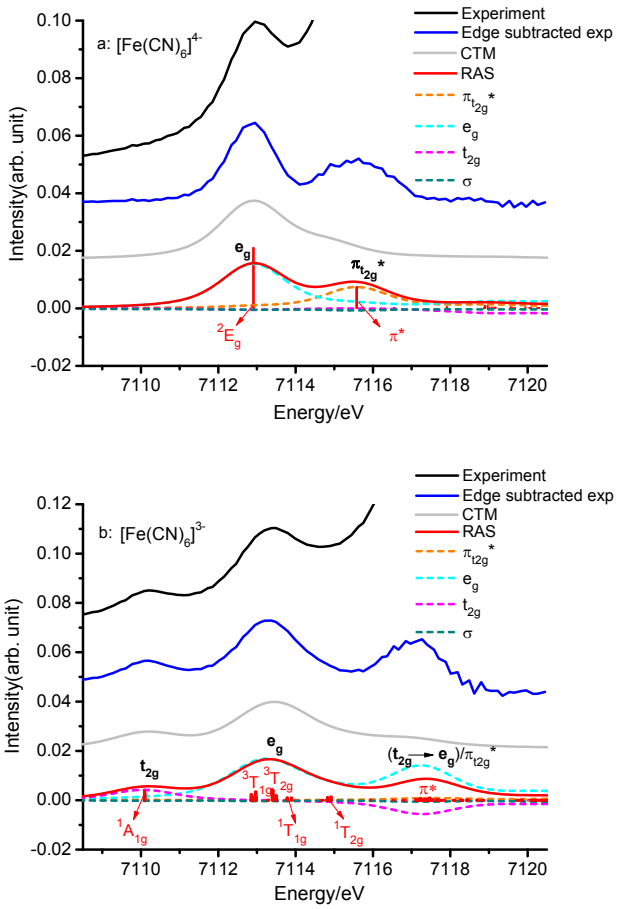

Fig. 6 Iron K pre-edge XAS spectra of (a) $[FeCN_6]^{4-}$ and (b) $[FeCN_6]^{3-}$ showing experimental data (black), the edge-subtracted spectra (blue), results from CTM calculations (light gray), and results from core RAS calculations (red). Analyses of the valence orbital contributions are shown as dashed lines.

detail in the next subsection.

The pre-edge spectrum of $[Fe(CN)_6]^{3-}$, with its $t_{2g}{}^5e_g{}^0$ ground-state configuration, is more complicated. At least two features are observed in experiment with an energy difference of 3.2 eV and an intensity ratio of 1.0:4.1.[7] In a ligand-field analysis, the first feature is an excitation to the t_{2g} orbital while the second one consists of a large number of different final states reached after excitation to the e_g orbitals, namely $^3T_{1g}$, $^3T_{2g}$, $^1T_{1g}$ and $^1T_{2g}$.[7,18] The relative position of these two features reflects the ligand-field strength. At the same time, the difference in energy between the T_{1g} and T_{2g} states probe the difference in attraction between the hole in a d_{xy} orbital and the electron in the d_{z2} compared to the d_{x2-y2}, the wavefunctions of $^3T_{1g}$ and $^3T_{2g}$ states are available in Fig. SI14. Again, this energy difference should depend on the orbital covalency.

The RAS calculations reproduces the 3.2-eV difference between the t_{2g} and e_g peaks, see Table 1, and gives a good overall shape of the spectrum, see Fig. 6. As for ferrocyanide, the total intensity is underestimated. The CTM calculation gives a very similar picture with an energy difference of 3.3 eV, and DFT gives a good energy splitting (3.5 eV) but a different structure of the e_g peak.[28] The RAS and CTM calculations also include a third peak, ∼4.0 eV above the e_g feature. This peak can also be seen in the edge-subtracted experimental spectrum. In analogy with the ferrocyanide assignment, this is likely to be a signature of π back-bonding. This is confirmed by a calculation without the π^* orbitals in the active space where the peak disappears, see Fig. SI15. However, the orbital analysis shows that he picture is more complicated, and the direct π^* excitation mixes with a $1s \rightarrow e_g + t_{2g} \rightarrow e_g$ shake-up excitation, see Fig. 6. If this mixing is excluded, the π^* peak still appears, but not until 13.6 eV above the e_g peak, see Fig. SI16.

If all pre-edge transitions could be resolved, their position would give information about both the ligand-field, the orbital covalency, and π back-donation. It should also be expected that the relative intensity of the t_{2g} and e_g features could be used to assign their relative covalency, in analogy to $[Fe(Cl)_6]^{3-}$. The experimental intensity ratio of 1.0:4.1 closely matches the number of t_{2g} and e_g holes (1:4), which suggests that the covalencies of these orbitals are similar. RAS predicts the e_g orbitals to be much more covalent than the t_{2g} orbitals, see Table SI 5, but still predicts an intensity ratio close to experiment (1.0:4.2). One possibility is that the intensity ratio is affected by other factors than the covalency, e.g., mixing with π^* configurations. Another possibility is that the lack of dynamical correlation in the RASSCF orbital optimization analysis affect the t_{2g} covalency more than the e_g covalency.

3.4 Comparing complexes

The six calculated complexes, in different ways, show how the K pre-edges are sensitive to oxidation state, ligand character, and coordination environment. The RAS model, which includes a balanced description of all relevant effects, accurately reproduces these changes. As an example, the energy splittings between major peaks are predicted with a mean absolute deviation (MAD) of only 0.1 eV. The CTM simulations give similar accuracy for the hexa-coordinate complexes, while TD-DFT gives reasonable ligand-field splittings, but larger deviations for systems where electron-electron interactions and multiple excitations contribute to the K pre-edge. In most cases, the relative intensities of different peaks are also well described by the RAS method. The possible exceptions are the three peaks in $[FeCl_6]^{4-}$, but that can possibly be assigned to an error in the experimental pre-edge fit.

The absolute transition energies are ∼20 eV too high in RAS, which is caused by the lack of core-hole relaxation. As described in the Computational details, all calculated spectra have therefore been shifted with an empirical parameter to improve the alignment. The important question is then the transferability of this parameter between complexes. When going from ferrous to ferric oxidation states the MAD is only 0.2 eV, see Table SI4. The energy shift is also relatively constant when changing the ligand. It is -18.4 eV for the four hexacoordinate complexes, with a MAD of 0.1 eV. However, for the two tetra-coordinate systems, the shift is larger -20.1 eV on average.

The relationships between the experimental and calculated values of the integrated pre-edge intensity are presented in Fig. 7. The agreement is very good for the four high-spin systems. This suggests that the core RAS method can reproduce intensity differences that come from changes in oxidation state or coordination environment during a reaction. It can be dangerous to assign much physical significance to a linear relationship between a small number of observations, but the calculations also reproduce another key experimental observation, the dipole/quadrupole ratios of the two tetrahedral complexes. This suggests that the RAS method can properly model the sensitive dipole contributions.

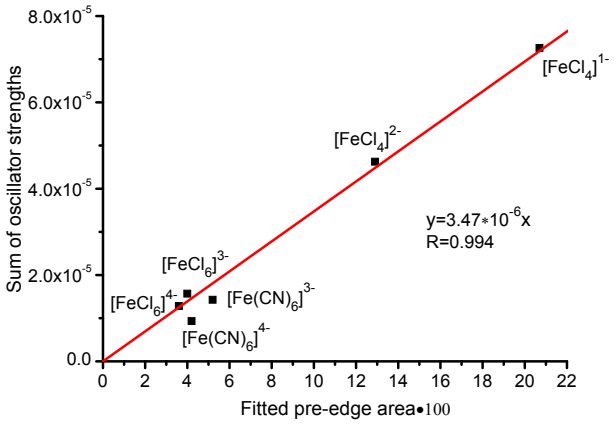

Fig. 7 Linear fit of the core RAS calculated intensities and the experimental K pre-edge intensities obtained from ref. [7].

In all three pairs, the pre-edge intensity is higher for the ferric compared to the ferrous complexes. In systems with only quadrupole transitions, this can partly be explained by an increase in the number of holes. For $[FeCl_4]^{n-}$, the explanation must be different because an extra hole in the e orbital would only have a small effect on the total intensity. Instead, the increased intensity comes from a higher degree of $3d$-$4p$ hybridization in the ferric system, 3.3%, compared to 2.1% for the ferrous complex.

In Fig. 7 the low-spin cyanide complexes deviate from the trend set by the high-spin chloride complexes. In both ferro- and ferricyanide, experiments predict higher pre-edge intensities than for the six-coordinated chloride complexes, while the calculations predict the opposite relationship. As an example, the experimental pre-edge area is 4.2 for $[Fe(CN)_6]^{4-}$ and 3.6 for $[FeCl_6]^{4-}$, see Table 1. Considering only the orbital covalencies, the result is surprising. In ferrocyanide, all four holes are in the covalent e_g orbitals while in ferrous hexachloride two of the holes are in weakly bonding t_{2g} orbitals and the other two are in e_g orbitals that are still less covalent than in ferrocyanide, see Table SI5. Consequently, both core RAS and DFT calculations predict higher intensity for the chloride compared to the cyanide complexes.[28] This means that either the calculations miss an important intensity mechanism, or that the experimental pre-edge areas of the cyanides have been overestimated in reference [7]. The problem does not seem to be the pre-edge fits, because the independent pre-edge fits in Figs. SI11-13 give similar results, see Fig. SI17.

The potential to extract electronic structure information depend on the ground-state electron configuration. The ligand-field strengths affect most of the spectra, and can be easily separated from the other interactions in the high-spin d^5 systems. Differential electron-electron repulsion can be used to probe orbital covalency for high-spin d^6 and low-spin d^5 systems. In all these systems, the difference in energy between $^1T_1$ and $^1T_2$ states depends on both t_{2g} and e_g covalency, and these effects cannot be separated only from the energies but requires an electronic structure model. For the high-spin d^6 systems, the energies are also affected by mixing with other configurations. The RAS model takes all these factors into account and give accurate estimates of relative peak energies.

The differences in orbital covalency between orbitals should also affect the relative intensities of different peaks. The analysis works best for the high-spin d^5 system in O_h symmetry, where there seems to be a linear relationship between covalency and peak intensity. A similar relationship could be expected for low-spin d^5 systems that also have non-interacting t_{2g} and e_g transitions. The relative intensities match the number of holes in the respective orbitals, which suggests that they have similar covalencies. For the d^6 systems in O_h symmetry, mixing of states from t_{2g} and e_g excitations makes the analysis more complicated. For the tetrahedral complexes, the covalency effects are dwarfed by the effects of electric dipole contributions.

For several complexes, both RAS and CTM models predict the presence of high-energy peaks obscured by the rising edge. In the ferric chloride complexes, these peaks are shake-up transitions of LMCT type. For the cyanide complexes, the high-energy peaks are associated with the empty π^* orbitals that are consequences of π back-bonding. Some of

these peaks can be preliminary identified already in the present spectra, but it would be interesting to see whether the theoretical predictions can be reproduced in higher quality data sets. That would prove the use of the RAS method to predict and interpret charge-transfer transitions in K-edge experiments, which opens up a new probe of metal-ligand orbitals.

4 Conclusions

The RAS method provides an accurate way to simulate K pre-edge spectra of a range of iron complexes with prototypical bonding situations. As shown by the calculations of the iron hexa-chlorides, it accurately includes both ligand-field and multiplet effects, as well as configuration interaction between different states. As shown by the iron tetrachlorides, the RAS calculations can also predict the relative intensity of electric quadrupole and electric dipole transitions from $3d$-$4p$ orbital hybridization in systems without an inversion center. This is important when studying changes in the coordination environment during a chemical reaction. This is difficult to model using the semi-empirical CTM model because adding $4p$ configurations significantly increases the number of fitting parameters. TD-DFT (BP86) includes the effects of orbital hybridization but overestimates the dipole contributions, at least for the current complexes modeled. RAS and CTM both predict charge-transfer features in the rising edges, some of which can be tentatively identified in the experimental spectra. The pre-edges contain information about both ligand-field strengths and orbital covalencies, which can be understood by analyzing the RAS wavefunction. The origin of different pre-edge features can also be explained using a graphic orbital analysis that serves as a bridge between spectra and electronic structure. This makes RAS an attractive method for the modeling of hard X-ray XAS and RIXS studies of many small and medium-sized transition-metal catalysts.

5 Acknowledgments

We thank Roland Lindh for help with integrals for electric octopoles and magnetic quadrupoles, and Per-Åke Malmqvist for valuable suggestions on the RAS calculations. We acknowledge financial support from the Marcus and Amalia Wallenberg Foundation, the Swedish Research Council, the Carl Trygger foundation, and the Knut and Alice Wallenberg Foundation for the project Strong Field Physics and New States of Matter (Grant No. KAW-2013.0020). The computations were performed on resources provided by SNIC trough Uppsala Multidisciplinary Center for Advanced Computational Science (UPPMAX) under project snic2013-1-317 and National Supercomputer Centre at Linköping University (Triolith) under project snic2014-5-36.

References

1 J. Yano and V. K. Yachandra, *Photosynth. Res.*, 2009, **102**, 241–254.
2 P. Glatzel, U. Bergmann, J. Yano, H. Visser, J. H. Robblee, W. Gu, F. M. de Groot, G. Christou, V. L. Pecoraro, S. P. Cramer and V. K. Yachandra, *J. Am. Chem. Soc.*, 2004, **126**, 9946–9959.
3 K. L. Stone, R. K. Behan and M. T. Green, *Proc. Nat. Acad. Sci. USA.*, 2005, **102**, 16563–16565.
4 J. Ward, E. Ollmann, E. Maxey and L. A. Finney, *L. A. Finney*, Springer, 2014, pp. 171–187.
5 J. Yano and V. Yachandra, *Chem. Rev.*, 2014, **114**, 4175–4205.
6 C. R. Randall, L. Shu, Y.-M. Chiou, K. S. Hagen, M. Ito, N. Kitajima, R. J. Lachicotte, Y. Zang and L. Que Jr, *Inorg. Chem.*, 1995, **34**, 1036–1039.
7 T. E. Westre, P. Kennepohl, J. G. DeWitt, B. Hedman, K. O. Hodgson and E. I. Solomon, *J. Am. Chem. Soc.*, 1997, **119**, 6297–6314.
8 F. M. de Groot, G. Vankó and P. Glatzel, *J. Phys-Condens. Mat.*, 2009, **21**, 104207.
9 F. A. Lima, T. J. Penfold, R. M. van der Veen, M. Reinhard, R. Abela, I. Tavernelli, U. Rothlisberger, M. Benfatto, C. J. Milne and M. Chergui, *Phys. Chem. Chem. Phys.*, 2014, **16**, 1617–1631.
10 A. Roe, D. Schneider, R. Mayer, J. Pyrz, J. Widom and L. Que Jr, *J. Am. Chem. Soc.*, 1984, **106**, 1676–1681.
11 S. DeBeer George, P. Brant and E. I. Solomon, *J. Am. Chem. Soc.*, 2005, **127**, 667–674.
12 T. Yamamoto, *X-Ray. Spectrom.*, 2008, **37**, 572–584.
13 J.-U. Rohde, T. A. Betley, T. A. Jackson, C. T. Saouma, J. C. Peters and L. Que, *Inorg. Chem.*, 2007, **46**, 5720–5726.
14 M. O. Krause and J. Oliver, *J. Phys. Chem. Ref. Data.*, 1979, **8**, 329–338.
15 P. Glatzel and U. Bergmann, *Coordin. Chem. Rev.*, 2005, **249**, 65–95.
16 P. Glatzel, M. Sikora and M. Fernández-García, *Euro. Phys. J. Spec. Top.*, 2009, **169**, 207–214.
17 P. Glatzel, T.-C. Weng, K. Kvashnina, J. Swarbrick, M. Sikora, E. Gallo, N. Smolentsev and R. A. Mori, *J. Electron. Spectrosc.*, 2013, **188**, 17–25.
18 M. Lundberg, T. Kroll, S. DeBeer George, U. Bergmann, S. A. Wilson, P. Glatzel, D. Nordlund, B. Hedman, K. O. Hodgson and E. I. Solomon, *J. Am. Chem. Soc.*, 2013, **135**, 17121–17134.
19 T. Kroll, R. G. Hadt, S. A. Wilson, M. Lundberg, J. J. Yan, T.-C. Weng, D. Sokaras, R. Alonso-Mori, D. Casa, M. H. Upton *et al.*, *J. Am. Chem. Soc.*, 2014, **136**, 18087–18099.
20 L. J. Ament, M. van Veenendaal, T. P. Devereaux, J. P. Hill and J. van den Brink, *Rev. Mod. Phys.*, 2011, **83**, 705.
21 B. M. Kincaid and P. Eisenberger, *Phys. Rev. Lett*, 1975, **34**, 1361.
22 H. Ågren, V. Carravetta, O. Vahtras and L. G. Pettersson, *Chem. Phys. Lett.*, 1994, **222**, 75–81.
23 L. Triguero, L. Pettersson and H. Ågren, *Phys. Rev. B*, 1998, **58**, 8097.
24 Y. Joly, *Phys. Rev. B*, 2001, **63**, 125120.
25 U. Ekström, P. Norman, V. Carravetta and H. Ågren, *Phys. Rev. Lett.*, 2006, **97**, 143001.
26 U. Ekström, P. Norman and V. Carravetta, *Phys. Rev. A*, 2006, **73**, 022501.
27 J. J. Rehr, J. J. Kas, F. D. Vila, M. P. Prange and K. Jorissen, *Phys. Chem. Chem. Phys.*, 2010, **12**, 5503–5513.
28 S. DeBeer George, T. Petrenko and F. Neese, *J. Phys. Chem. A.*, 2008, **112**, 12936–12943.
29 P. Chandrasekaran, S. C. E. Stieber, T. J. Collins, L. Que Jr, F. Neese and S. DeBeer George, *Dalton. T.*, 2011, **40**, 11070–11079.
30 F. A. Lima, R. Bjornsson, T. Weyhermüller, P. Chandrasekaran, P. Glatzel, F. Neese and S. DeBeer George, *Phys. Chem. Chem. Phys.*, 2013, **15**, 20911–20920.
31 A. Dreuw, J. L. Weisman and M. Head-Gordon, *J. Chem. Phys.*, 2003, **119**, 2943–2946.
32 S. DeBeer George, T. Petrenko and F. Neese, *Inorg. Chim. Acta.*, 2008,

361, 965–972.

33 G. Capano, T. Penfold, N. Besley, C. Milne, M. Reinhard, H. Rittmann-Frank, P. Glatzel, R. Abela, U. Rothlisberger, M. Chergui and I. Tavernelli, *Chem. Phys. Lett.*, 2013, **580**, 179–184.

34 F. M. de Groot, *Coordin. Chem. Rev.*, 2005, **249**, 31–63.

35 E. C. Wasinger, F. M. de Groot, B. Hedman, K. O. Hodgson and E. I. Solomon, *J. Am. Chem. Soc.*, 2003, **125**, 12894–12906.

36 R. K. Hocking, E. C. Wasinger, F. M. de Groot, K. O. Hodgson, B. Hedman and E. I. Solomon, *J. Am. Chem. Soc.*, 2006, **128**, 10442–10451.

37 R. K. Hocking, E. C. Wasinger, Y.-L. Yan, F. M. deGroot, F. A. Walker, K. O. Hodgson, B. Hedman and E. I. Solomon, *J. Am. Chem. Soc.*, 2007, **129**, 113–125.

38 M.-A. Arrio, S. Rossano, C. Brouder, L. Galoisy and G. Calas, *Europhys. Lett.*, 2000, **51**, 454.

39 P.-Å. Malmqvist, A. Rendell and B. O. Roos, *J. Phys. Chem.*, 1990, **94**, 5477–5482.

40 N. Engel, S. I. Bokarev, E. Suljoti, R. Garcia-Diez, K. M. Lange, K. Atak, R. Golnak, A. Kothe, M. Dantz, O. Kuhn *et al.*, *J. Phys. Chem. B.*, 2014, **118**, 1555–1563.

41 R. V. Pinjari, M. G. Delcey, M. Guo, M. Odelius and M. Lundberg, *J. Chem. Phys.*, 2014, **141**, 124116.

42 R. V. Pinjari, M. G. Delcey, M. Guo, M. Odelius and M. Lundberg, *J. Comput. Chem.*, 2015.

43 P.-Å. Malmqvist, K. Pierloot, A. R. M. Shahi, C. J. Cramer and L. Gagliardi, *J. Chem. Phys.*, 2008, **128**, 204109.

44 F. Aquilante, L. De Vico, N. Ferré, G. Ghigo, P.-Å. Malmqvist, P. Neogrády, T. B. Pedersen, M. Pitoňák, M. Reiher, B. O. Roos, L. Serrano-Andrés, M. Urban, V. Veryazov and R. Lindh, *J. Comput. Chem.*, 2010, **31**, 224–247.

45 K. Pierloot, *Mol. Phys.*, 2003, **101**, 2083–2094.

46 B. O. Roos, R. Lindh, P.-Å. Malmqvist, V. Veryazov and P.-O. Widmark, *J. Phys. Chem. A.*, 2004, **108**, 2851–2858.

47 B. O. Roos, R. Lindh, P.-Å. Malmqvist, V. Veryazov and P.-O. Widmark, *J. Phys. Chem. A.*, 2005, **109**, 6575–6579.

48 F. Aquilante, T. B. Pedersen and R. Lindh, *J. Chem. Phys*, 2007, **126**, 194106.

49 F. Aquilante, P.-Å. Malmqvist, T. B. Pedersen, A. Ghosh and B. O. Roos, *J. Chem. Theory. Comput.*, 2008, **4**, 694–702.

50 G. Ghigo, B. O. Roos and P.-Å. Malmqvist, *Chem. Phys. Lett.*, 2004, **396**, 142–149.

51 N. Forsberg and P.-Å. Malmqvist, *Chem. Phys. Lett.*, 1997, **274**, 196–204.

52 S. Bernadotte, A. J. Atkins and C. R. Jacob, *J. Chem. Phys.*, 2012, **137**, 204106.

53 J. Overgaard, H. Svendsen, M. A. Chevalier and B. B. Iversen, *Acta. Crystallorg. E.*, 2005, **61**, 268–270.

54 J. K. Beattie and C. J. Moore, *Inorg. Chem.*, 1982, **21**, 1292–1295.

55 Z. Warnke, E. Styczeń, D. Wyrzykowski, A. Sikorski, J. Kłak and J. Mroziński, *Struct. Chem.*, 2010, **21**, 285–289.

56 J. W. Lauher and J. A. Ibers, *Inorg. Chem.*, 1975, **14**, 348–352.

57 J. Kuchar, J. Cernak and W. Massa, *Acta. Crystallorg. C.*, 2004, **60**, 418–420.

58 A. D. Becke, *Phys. Rev. A*, 1988, **38**, 3098.

59 J. P. Perdew, *Phys. Rev. B*, 1986, **33**, 8822.

60 F. Neese, *Inorg. Chim. Acta*, 2002, **337**, 181–192.

61 A. D. Becke, *J. Chem. Phys.*, 1993, **98**, 5648–5652.

62 M. Frisch, G. Trucks, H. Schlegel, G. Scuseria, M. Robb, J. Cheeseman, G. Scalmani, V. Barone, B. Mennucci, G. Petersson *et al.*, *Gaussian Inc.: Wallingford, CT, USA*, 2009.

63 T. Lu and F. Chen, *J. Comput. Chem.*, 2012, **33**, 580–592.

64 G. N. George and I. J. Pickering, in *G. N. George and I. J. Pickering*, Exafspak: A Suite of Computer Programs for Analysis of X-ray Absorption Spectra;Stanford Synchrotron Radiation Laboratory: Stanford, CA, 2000.

65 M. H. Lim, J.-U. Rohde, A. Stubna, M. R. Bukowski, M. Costas, R. Y. Ho, E. Münck, W. Nam and L. Que, *Proc. Nat. Acad. Sci. USA.*, 2003, **100**, 3665–3670.